CONTINUOUS CASTING OF STEEL: COMPUTATIONAL MODELING AND VALIDATION

Brian G. Thomas, Hyun-Jin Yang[1], Seong-Mook Cho[2], and Matthew L.S. Zappulla[3]
Department of Mechanical Engineering,
Colorado School of Mines, Golden, CO, USA
(1. Graduate student, University of Illinois, Urbana, IL, USA;
2. Postdoctoral Researcher; CSM. 3. Graduate student, CSM)
Corresponding author's e-mail: bgthomas@mines.edu

Abstract: Computational models can help to understand and improve complex mature processes such as continuous of steel in many ways, including understanding the mechanisms of defect formation. This requires rigorous validation with experimental measurements to demonstrate that the models sufficiently capture the important phenomena that govern the behaviors of interest, are formulated correctly, and have accurate property data. This work reviews a few examples of computational models and their validation with experiments from the authors' recent research. Turbulent flow predictions are validated with measurements of gas pockets inside the nozzle and resulting bubble size distributions in the mold. Predicted surface velocity and level profiles and their fluctuations are compared with plant measurements using nailboards. Finally, the shape of longitudinal depressions predicted with a thermal-mechanical model are compared with micrographs in cast slabs. The capabilities of advanced modern computational models to match real-world measurements continues to improve.

Keywords: Continuous casting, computational models, measurements, validation

1. Introduction

The steel continuous-casting process and the digital computer appeared at about the same time in history. Continuous casting has grown to produce over 95% of steel in the world[1]. Similarly, computational modelling has grown due to tremendous advances in computer power and to great improvements in the sophistication of modelling software. During most of this time, advances to steel continuous casting were accomplished mainly by logically-based plant experiments, with input from laboratory experiments. As the process has become more mature, however, and problems become more difficult to understand and solve by trial and error, computational models can play an increased role in current and future advances.

Computational models can help to improve a process in many ways. Online models can control the process in real time, such as the control of secondary spray cooling using dynamic heat conduction models[2]. Semi-online models can provide efficient feedback to operators and engineers, to enable them to trouble-shoot the cause of problems and to find solutions[3]. Finally, advanced offline models, the subject of this paper, can capture complex coupled phenomena to realistically simulate the process. Such models can reveal new insights into understanding the process, such as explaining the mechanism(s) of how a particular defect likely formed.

After development of a computational model, it should be verified with known analytical solutions to show that it was formulated correctly, and that numerical errors are managable. Next, validation with experimental measure-ments is critical, to ensure that the model assumptions are reasonable, that the model captures all of the phenomena important to the problem of interest, and that the constants and property data in the model are sufficiently accurate. This paper summarizes a few examples involvingvalidation of computational models of continuous casting with measurements, focusing on recent research by the authors.

2. Continuous-Casting Phenomena

Like all real-world processes, continuous casting is tremendously complex, with a wide range of coupled phenomena, that interact over a vast range of time and size scales. Some of these phenomena include:

- turbulent, multiphase, transient fluid flow in a complex geometry (inlet nozzle and strand liquid pool), as affected by argon gas bubbles, electromagnetic forces, thermal, and solutal buoyancies
- injection of argon gas that forms large gas pockets and bubbles, their coalescence and breakup as they are transported through the turbulent flowing liquid, and their influence on the flow pattern and possible entrapment into the solidifying steel
- dynamic motion of the free liquid surfaces and interfaces between many different phases, including the effects of surface tension, oscillation, gravity-induced waves, and fluid momentum
- thermodynamic, thermal, and mechanical interaction within and between the atmosphere, powder / slag phases, refractory walls, and the different steel phases, including reoxidation, and the generation of indigenous and exogenous inclusions, liquid and solid precipitates
- conduction, convection, radiation, and thermodynamic reactions within the heating, melting, sintering, flowing, thickening, and crystallizing powder / slag phases.
- flow and heat transport in the liquid and solid flux layers, which float on the top surface of the steel
- transport of superheat in the turbulent steel
- transport of solute (including intermixing during a grade change) in the turbulent steel
- transport of complex-geometry inclusions through the liquid, including the effects of buoyancy, turbulent interactions, agglomeration, and possible entrapment of the inclusions on nozzle walls, gas bubble surfaces, dendritic steel solidification front, and the top surface meniscus
- thermal, fluid, and mechanical interactions in the meniscus region between the solidifying meniscus, solid slag rim, infiltrating molten flux, liquid steel, powder layers, and inclusion particles.
- heat transport through the solidifying steel shell, the interface between the shell and mold, (which contains powder layers and growing air gaps) and the copper mold.
- mass transport of crystallizing slag down the interfacial gap between shell and mold.
- thermal distortion, wear, and forces applied by the mold walls and the support and drive rolls
- nucleation and growth of solid crystals, both in the melt and against solid surfaces, and their transport through the flowing melt pool
- solidification of the steel shell, including the growth of dendrites, grains and complex microstructures, multi-component phase transformations, precipitate formation, and microsegregation.
- shrinkage of the solidifying steel shell, due to thermal contraction, phase transformations, and internal stresses.
- stress generation within the solidifying steel shell, due to external forces, (friction with the mold walls, bulging between the support rolls, withdrawal, gravity) thermal strains, creep, and plasticity (which varies with temperature, grade, and cooling rate)
- crack formation, due to the combined interactions of fluid flow, porosity nucleation, heat transfer, stress, and microstructure evolution.
- coupled segregation, on both microscopic and macroscopic scales

3. Multiphase Flow in Nozzle and Mold

Turbulent fluid flow in the nozzle and mold is greatly important to steel quality. To reduce nozzle clogging problems, for example, argon gas is often injected into various places inside the nozzle. The injected gas interacts with the liquid steel flow in a complex manner to produce a size distribution of bubbles exiting the nozzle into the mold. The bubbles greatly affect the flow pattern and may cause serious defects if captured into the solidifying shell. This gas may also may accumulate into gas pockets inside the nozzle, which can be sheared intermittently into large bubbles, and greatly affect both the flow pattern and the flow stability of the system. These

phenomena are difficult for conventional computational fluid dynamics models to capture.

A new EEDPM hybrid model is being developed to simulate these phenomena[4,5]. It couples together an Eulerian-Eulerian (EE) model of the liquid steel and argon phases including the gas fraction field, together with a Discrete Phase Model (DPM) of particle (gas bubble) transport. The EE model identifies regions of high gas fraction where gas pockets form, typically where there is recirculating flow. The DPM model solves for the transport, breakup, and coalescence of the bubbles through the EE velocity field, and tracks their evolving size distribution. Bubbles are generated in the DPM model according to a shearing detachment criterion at the bottom of the gas pockets calculated in the EE model. The DPM model provides the needed bubble size for the EE model. Mass balance is easily satisfied independently in both models, because there is no mass exchange between the models. The EEDPM model has been implemented into the commercial CFD software ANSYS-Fluent[6] via extensive UDF user subroutines.

The new EEDPM model has been applied to simulate turbulent flow in several relevant benchmark experiments, including air bubble transport in turbulent water flow in vertical pipes[7], and argon / molten Galinstan metal flow in a model caster[8]. The latter experiment is like a stopper-rod, nozzle, and mold system, but has a very thin geometry, to enable x-ray visualization. This exaggerates the effects of gas surface tension and gas pocket formation, so is a more difficult test of the new EEDPM model than the real process. Fig. 1 shows sample results comparing the gas fractions in the nozzle region between the hybrid model simulation and x-ray visualization of the lab experiment[8].

The simulation and measured results both show that three gas pockets form near the nozzle top: at the stopper tip and at each side wall, with periodic oscillation of the gas pockets and velocity fields. Furthermore, the side gas pockets are observed to shed bubbles periodically from below.

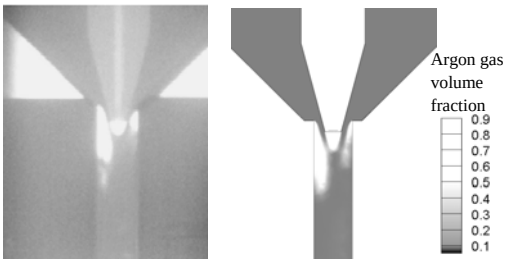

Figure 1 Comparison of measurement (left) and simulation (right) of gas pocket shape inside nozzle

The bubble size distribution evolves as the bubbly molten steel flow in the nozzle exits into the mold. The strong jets from the ports expand quickly to span the entire thickness of the thin mold, traverse across to impinge on the narrow-face mold walls, and divide upwards and downwards. Bubbles entrained with the upward flow can escape from the top surface of the mold, so only a few are observed. Bubbles entrained with the downward flow are mostly trapped beneath the jet, as the jet obstructs their path to float upwards. Some bubbles escape down from the bottom of the mold, but most accumulate below the jet and coaelesce into larger bubbles as they circulate in the lower region of the mold. Experimental observations report the same phenomenon that only a few bubbles rise directly toward the top surface, and most bubbles are found in the lower region of the mold below the nozzle port.

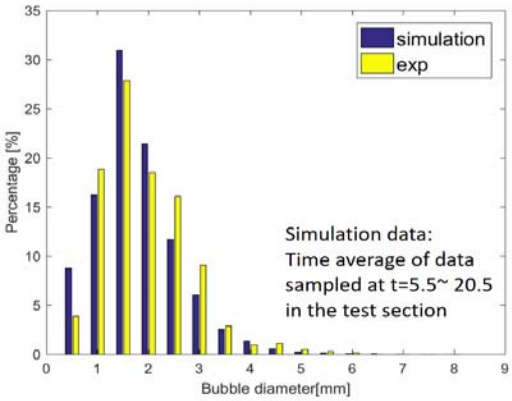

Figure 2 Comparison of predicted bubble size distribution with measurements

Fig. 2 compares the bubble size distribution in the mold from the EEDPM model with the

corresponding measurements. The model only slightly underpredicts the measurements.

4. Surface Velocity and Level Profiles and Their Variations

Behavior of the top surface of the molten steel in the mold is very important to the quality of continuous-cast steel. If the surface velocities are too high, mold slag can be entrained, leading to inclusion and sliver defects in the product. If the surface level profile is too steep, insufficient mold slag may be consumed into the interfacial gap between the solidifying steel shell and the mold, leading to lubrication problems, thermal variations, and surface cracks, especially where the level is too high. If the surface level experiences excessive fluctuations, initial solidification at the meniscus can be disrupted, leading to surface defects such as entrained mold slag and slivers.

Computational models of turbulent flow in the nozzle and mold can be easily extended to predict these important surface phenomena. After solving the mass and momentum transport equations, simple models with a flat top surface can convert the calculated pressure variations into surface level variations via a potential energy balance[9]. When surface level fluctuations involve complicated surface waves or sloshing, etc., more advanced free surface methods can be applied.

An important measurement tool for gaining validation data for model predictions of fluid flow in the mold is to insert nails or nail boards into the top surface down through the slag layer. With proper insertion time, ~3s, a small lump of steel will solidify onto the nail tip. This method was pioneered to measure the thickness of the liquid slag layer that floats above the steel, by comparing with corresponding aluminum wires. Recently, a new methodology has been found to estimate the liquid slag layer depth directly from the color profile of the scale along the nail[10].

Nails provide several more important ways to validate flow model predictions. By observing the variations in the run-up height around the nail, the direction of the flow can be determined. Furthermore, by analyzing the run-up height, the velocity of the molten steel past the nail can be found[11]. Fig. 3 compares such measurements of surface velocity and direction with calculations from a model of multiphase flow in a slab caster[12]. These results show a strong cross-flow from the inside to the outside radius. This was caused by the slide-gate opening near the inside radius side of the nozzle generating swirl that led to argon gas exiting the nozzle ports towards the inside-radius in the mold, and then buoying the flow there upwards[12].

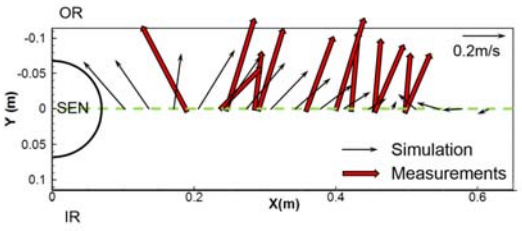

Figure 3. Surface velocity along centerline comparing model predictions and nail-board measurements

By comparing the lump positions of a series of nails attached to an inserted nail board, the surface level profile across the top of the caster can be found[11]. Examples of both surface velocity profiles and surface level profiles from 10 such nailboard experiments are compared with results of Large Eddy Simulations (LES) in Figs. 4 and 5[9]. The time averages of both profiles match well with the average of the measurements[9]. This work further reveals insight into their time variations, which also match well with the corresponding measurements. Specifically, the predictions show that times with higher surface velocity, and more severe variations of the surface level profile, both correspond with clockwise flow of the swirling jets exiting the nozzle ports. This was associated with strong flow directly down from beneath the slide-gate opening, and down the outside-radius-side of the nozzle. Time intervals with lower velocity generally correspond with counter-clockwise nozzle swirl, which was associated with flow inside the nozzle crossing over to the inside-radius side. This crossover slows the jet, leading to weaker jets exiting the ports, and

slower surface velocities a short time interval later, according to the time needed for the flow to reach the narrow face, and deflect upwards to the top surface. This work shows the importance of the flow-control device (slide gate or stopper rod) on surface velocity variations in the mold. It suggests that control of flow variations inside the nozzle could help to stabilize flow in the mold and surface[9].

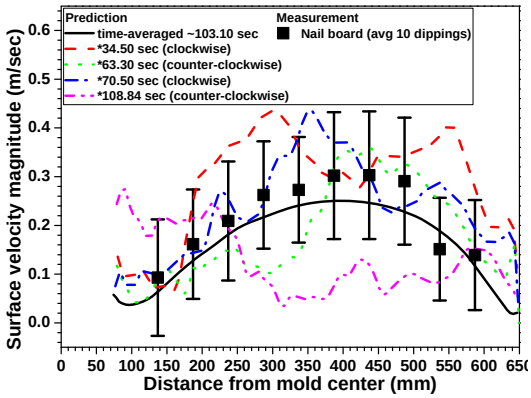

Figure 4. Surface velocity profiles and variations comparing LES model and nail-board measurements

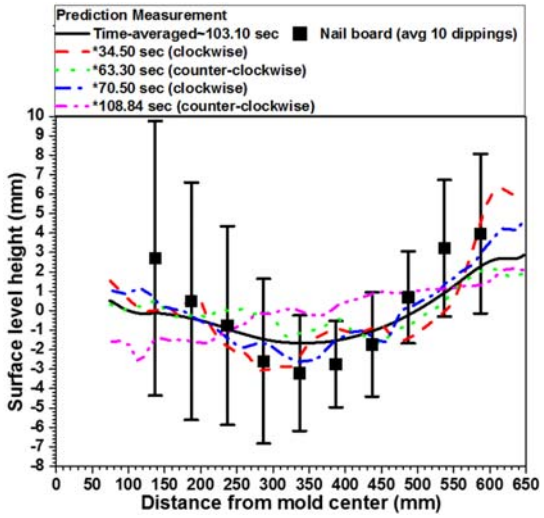

Figure 5. Surface level profiles and variations comparing LES model and nail-board measurements

5. Heat Transfer and Breakout Shells

Heat transfer is the most basic phenomenon to control in continuous casting, and problems such as local drops in mold heat transfer can lead to breakouts. Transient heat-transfer solidification models can be validated with measurements of mold heat flux from heatup of the cooling water, and with temperature measurements from thermocouples in the mold walls. Further validation is possible from comparison of the solidified shell thickness with breakout shells [13].

An example comparing model predictions with measurements around the perimeter of a breakout shell from a beam-blank caster are shown in Fig. 6[13]. The variations depend on both the drop in heat transfer due to gap formation between the shell and the mold wall in the shoulder region, due to excessive flange taper predicted with a thermal-mechanical model[13], and the additional effect of superheat delivery from the turbulent flow, included in a multiphysics model[13].

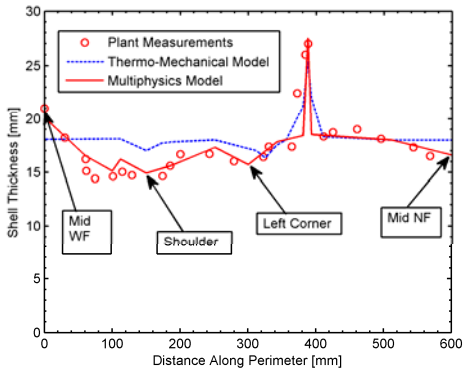

Figure 6. Model predictions and measurements of breakout shell thickness in a beam-blank caster

6. Longitudinal Depressions

Crack formation is another serious defect in continuous casting. Internal hot-tear cracks fill with interdendritic liquid to cause macrosegregation which cannot be removed, while surface defects oxidize, leading to slivers during rolling. Surface cracks are often accompanied by depressions. Thermal-mechanical models are being applied to simulate phenomena such as the formation and growth of depressions and cracks[14].

The first step is validation of the heat transfer model[15], which includes a detailed treatment of the gap, including separate thermal resistances for the slag layers, air gap and contact resistances[14]. The mechanical model can be validated by comparison with the shape of the simulated

depressions. For example, Fig. 7 shows a longitudinal depression during solidification that was simulated by applying 7.5% tensile strain over 30s starting when the shell was 3mm thick. The depression forms due to necking of the thinnest part of the shell in the mold, caused by a thermal-mechanical instability. Specifically, the depression causes a local drop in heat transfer across the interfacial gap. This leads to a hotter, thinner shell beneath the depression, where strain concentrates when a tensile load is applied. The predicted depression depth is similar to that observed in a micrograph of a depression with a crack in the final solidified steel slab[14]. The depression shape does not exactly match the micrograph, likely due to changes in shape during deformation in the rest of the caster, and also from the possible influence of the crack on the shape evolution. This model is being applied to correlate the shape of depressions with the mechanism of their formation. Ultimately, the goal is to relate shape of the surface depressions to the mechanism of crack formation, and identify effective practice(s) to correct the problems.

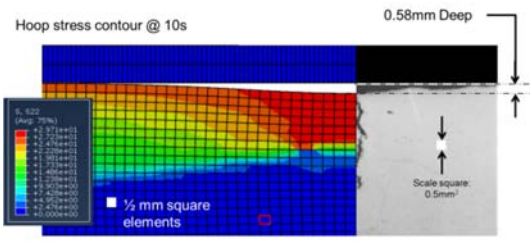

Figure 7 Simulated longitudinal depression shape (with transverse stresses) compared to micrograph

7. Conclusions

Computational models have great potential to increase understanding and enable improvements to mature manufacturing processes, such as continuous casting of steel. To be useful, however, the models must include all of the important phenomena that govern the behaviors of interest, which are not always obvious. Thus, model validation with experimental measurements is essential. This paper has shown a few examples of such validation, relevant to fluid flow in the nozzle and mold, surface profile and level fluctuations, the formation of breakouts due to shell thinning in the mold, and longitudinal depressions. As computational models continue to improve, and to better match with measurements, they should lead to further advances in the continuous casting process.

Acknowledgements:
Support of this work from the Continuous Casting Consortium at the University of Illinois, Urbana, IL, USA, the Continuous Casting Center at the Colorado School of Mines, Golden, CO, USA, and the National Science Foundation (Grant CMMI 15-63553) is gratefully acknowledged.

References:

[1] *World Steel in Figures 2016*, World Steel Association, worldsteel.org: 2016, p1.
[2] B. Petrus, K. Zheng, X. Zhou, B.G. Thomas and J. Bentsman: Metall. Mater. Trans. B, Vol. 42 (1), 2011, p87.
[3] B. G. Thomas: Iron & Steel Technology. 2010, Vol. 7 (7), p70.
[4] H.-J. Yang and B. G. Thomas: *SteelSim 2017*, Qingdao, PR China, 2017.
[5] H.-J. Yang, S. P. Vanka and B. G. Thomas: ASME IMECE2017, Tampa, Florida, USA, 2017.
[6] Ansys FLUENT, Release 16.2. Ansys Inc., Canonsburg, PA, www.ansys.com: 2016.
[7] T. Hibiki, M. Ishii, and Z. Xiao: Int. J. of Heat and Mass Transfer, Vol. 44 (10), 2001, p1869.
[8] K. Timmel, N. Shevchenko, M. Röder, M. Anderhuber, P. Gardin, S. Eckert, and G. Gerbeth: Metall. Mater. Trans. B, Vol. 46 (2), 2015, p700.
[9] S. M. Cho, B. G. Thomas and S. H. Kim: Metall. Mater. Trans. B, Vol. 47 (5), 2016, p3080.
[10] A. Akhtar, B.G. Thomas and J. Sengupta: *AISTech 2016*, Pittsburgh, PA, 2016, p1427.
[11] R. Liu, B.G. Thomas, J. Sengupta, S.D. Chung and M. Trinh: ISIJ Internat., Vol. 54 (10), 2014, p2314.
[12] K. Jin, B.G. Thomas and X.M. Ruan, Metall Mater Trans B. Vol. 47 (1), 2016, p548.
[13] S. Koric, L. C. Hibbeler, R. Liu and B. G. Thomas: Numer Heat Transfer B-Fund. Vol. 58 (6), 2010, p371.
[14] M.L. Zappulla and B.G. Thomas: TMS Annual Meeting, Supplemental Proceedings, 2017, p501.
[15] M.L. Zappulla, B.G. Thomas and L. Hibbeler: Metall. Mater. Trans. A. Vol. 48 (8), 2017, p3777.